2014

Viruses as nanoparticles: Structure *versus* collective dynamics

S. Sirotkin
Universite de Lyon

A. Mermet
Universite de Lyon

M. Bergoin
Universite Montpellier

V. Ward
University of Otago

James L. Van Etten
University of Nebraska-Lincoln, jvanetten1@unl.edu

Viruses as nanoparticles: Structure *versus* collective dynamics

S. Sirotkin,[1] A. Mermet,[1] M. Bergoin,[2] V. Ward,[3] and J. L. Van Etten[4]

[1]*Institut Lumière Matière, Université de Lyon, Université Claude Bernard Lyon 1, UMR CNRS 5306, 69622 Villeurbanne, France*

[2]*Laboratoire de Virologie Comparé des Invertébrés, E.P.H.E., Université Montpellier 2, France*

[3]*University of Otago, Department of Microbology and Immunology, New Zealand*

[4]*Department of Plant Pathology and the Nebraska Center for Virology, University of Nebraska-Lincoln, Lincoln, Nebraska USA*

(Received 21 May 2014; revised manuscript received 7 August 2014; published 27 August 2014)

In order to test the application of the "nanoparticle" concept to viruses in terms of low-frequency dynamics, large viruses (140–190 nm) were compared to similar-sized polymer colloids using ultra-small-angle x-ray scattering and very-low-frequency Raman or Brillouin scattering. While both viruses and polymer colloids show comparable highly defined morphologies, with comparable abilities of forming self-assembled structures, their respective abilities to confine detectable acoustic vibrations, as expected for such monodisperse systems, differed. Possible reasons for these different behaviors are discussed.

DOI: 10.1103/PhysRevE.90.022718 PACS number(s): 87.64.kp, 62.25.−g, 63.22.−m, 87.15.H−

I. INTRODUCTION

There is an increasing interest to use viruses as particles that offer nanospecific properties that may compete with polymer or inorganic colloids [1–5]. Most imaging experiments such as atomic force microscopy (AFM) [6] or cryoelectron microscopy (cryoEM) [7] indicate that viruses have highly defined and stable morphologies. Scanning force microscopy has unveiled the remarkable toughness of some virus shells [8,9], which can be used for a variety of applications. Given the combination of morphological compactness and relatively high toughness, it is tempting to consider paraspherical viruses as nanospheres similar to polymer or inorganic nanoparticles; as such, they are expected to confine acoustic vibrations in the form of global collective motions. Such types of vibrations [10], also called nanoparticle modes, are valuable probes of nano-objects as they provide information on their overall dynamical collective behavior [11–13]. At stake, in the case of viruses, is the characterization of the role played by global vibrations in the large scale conformational changes (like the compact-swollen transition) during their life cycles [14,15] or possibly in their activity.

A common technique to probe nanoparticles modes is low-frequency Raman or Brillouin scattering. Attempts to probe nanoparticle modes from viruses using this technique are rare [16–18], thereby calling for more experimental exploration. In particular, the linear relationship between frequency and inverse size, that is the irrefutable signature of nanoparticle modes[19], has not yet been established for viruses. On the other hand, several computational studies performed on different paraspherical viruses have identified nanoparticle modes in viruses [15,20,21] so that it can still be considered a challenge to unambiguously detect them. One major difficulty in low-frequency inelastic light scattering from biological objects arises from the presence of water, for essentially two reasons: (i) water, as a bulk embedding medium, yields a broad quasielastic signal that screens all possible underlying weaker inelastic signals from lower concentration species (this situation also occurs when investigating solid nanoparticles in solutions); (ii) water is chemically part of the virus structure and thus might cause severe vibrational damping. So far, the effect of damping on the vibration modes of viruses has only been investigated theoretically [22–24]. These studies indicate that not all nanoparticle modes are equally affected by damping, so that the least damped ones should be the less symmetric modes with $\omega\tau$ values close to unity.

The purpose of the present paper is to investigate the different behaviors of soft viral nanospheres versus their hard polymer counterparts, particularly upon the progressive removal of their native solvents. In contrast to previous studies [16], the larger sizes of the current viruses are in a range for which the inelastic light-scattering selection rules are less restrictive than what they are for smaller sizes (i.e., sizes much smaller than the wavelength of the exciting laser), thus potentially more open to nanoparticle mode detection. To substantiate the morphological similarity between the viruses in this study and polymer nanospheres, we first report ultra-small angle x-ray scattering (USAXS) comparisons of both systems. In the second part of the paper, the Raman and Brillouin data of both systems are compared and discussed.

II. SAMPLES AND EXPERIMENTAL MEASUREMENTS

A. Samples

Three viruses were studied: Paramecium Bursaria Chlorella Virus type 1 (PBCV-1) and the invertebrate iridescent viruses IIV-6 [Chilo Iridescent Virus (CIV)] and IIV-9 [Wiseana Iridescent Virus (WIV)].

PBCV-1 is a double-stranded DNA virus that infects certain green algae; its structure is icosahedral with vertex-to-vertex diameter of 190 nm [25–27]. PBCV-1 has a few external fibers on the surface of the particle and one vertex has a 56-nm spike of which 34 nm protrudes from the surface [28]. CIV and WIV are insect viruses with double-stranded DNA genome. They both feature icosahedral shapes with 185-nm [27,29] and 140-nm diameter [30], respectively. Fibrillar structures cover the surfaces of both iridoviruses, but unlike PBCV-1, all their vertices are believed to be identical. The virus aqueous suspensions were a 50-mM Tris buffer with 5-mM $MgCl_2$ for PBCV-1, while the CIV and WIW suspensions contained 0.01 mol% azide.

The reference polymer colloid chosen for the study is polystyrene (PS) nanospheres purchased from Merck (grade

Estapor) with a declared diameter of 187 nm and standard deviation lower than 5%. The PS colloids are produced in an aqueous buffer.

To reduce the aqueous contribution as much as possible for the low-frequency Raman experiments, the particle suspensions were centrifuged at 23 000g for 30 min to produce pellets. As expected the two iridovirus pellets and the PS pellets had opal tints, indicating the formation of 3D paracrystalline arrays. Interestingly, the PBCV-1 pellets remained white.

B. USAXS measurements

The USAXS measurements compared the overall morphologies of the three viruses with those of the PS microspheres; the measurements were not intended to provide a quantitative detailed structural analysis of the viruses.

The measurements were performed at the ID02 beamline of the European Synchrotron Radiation Facility (Grenoble, France). The operating energy was 12.5 keV, for a photon flux of 10^{13} photons per second and an image plate detector positioned at 10 m from the sample. Typical integrated exposure times did not exceed 1s, to minimize radiation damage. The beam size was 0.3 by 0.8 mm^2 and samples were measured using a flow-through capillary. All displayed spectra result from an average of ten spectra recorded at different sample points illuminated during 0.05 or 0.06 seconds. The spectra were normalized to the intensity of the incident beam and scattering from the background (buffer + capillary) was subtracted.

C. Raman and Brillouin measurements

Since the nanoparticle modes of interest have typical frequencies lower than 1 cm^{-1} (i.e. 30 GHz), the low frequency inelastic light scattering experiments were performed using a multipass tandem Fabry-Perot interferometer [31]. The samples were illuminated with the 532 nm line of a diode pumped solid state compact laser, with a power no greater than 10 mW, to minimize possible radiation damage. The sample pellets were placed either in capillaries or in between coverslips; all measurements were made in backscattering geometry and at room temperature. Parallel (VV) and crossed (VH) polarization spectra were achieved by placing a grid polarizer with polarization axis oriented respectively either parallel or normal to the incident laser polarization, in a collimated path of the scattered light.

D. TEM and AFM measurements

The TEM observations were made after depositing a drop of the diluted suspensions on copper grids and after letting the drops dry in air for 24 H. For the virus samples, images were made in negative staining, using uranyl acetate. The AFM observations were made after depositing a drop of a fresh CIV pellet on a Si wafer; the pellet was observed to dry off very quickly under the influence of the while light used in the experiment. Measurements were made in tapping mode with a 15 nm Si tip. All measurements were made at room temperature.

III. RESULTS AND ANALYSIS

A. USAXS characterization

CIV, PBCV-1, and PS samples were characterized both in the form of diluted suspensions and as pellets. In diluted conditions, the collected information pertains to the individual noninteracting nanoparticles (form factor), while the study of the pellets characterizes the self-assemblies. USAXS data for WIV can be found in Ref. [30].

1. Diluted suspensions

Figure 1 displays the azimuthally averaged isotropic USAXS profiles of CIV, PBCV-1, and PS nanospheres, over the 0.01–0.5 nm^{-1} Q-wave vector range. The three profiles feature well-pronounced oscillations that are typical of spherical morphologies. While the profile of the PS nanospheres fits well with the form factor of hard spheres (with a diameter D of 188 $\pm$ 1 nm), the spherical core-shell model better captures the main features of the virus profiles. The core-shell sizes obtained for the fits shown in Fig. 1 are 66-5 (radius-thickness) nm and 77-6 nm for CIV and PCBV-1, respectively. The relatively poor agreement between the experimental curves and the fit curves in the first few oscillations between 0.05 and 0.1 nm^{-1} is most likely due to the inadequacy of the spherical form factor in describing an actual icosahedral viral morphology. In the case of CIV, this situation might be worse due to the known complex inner double shell structure of the virus [27,29]. Yet, the obtained sizes qualitatively agree with those derived from cryoEM [27]. In terms of polydispersities, both viruses and PS nanospheres are highly monodisperse systems, as shown by the numerous high-Q oscillations.

2. Pellets

Figure 2 displays the 2D USAXS patterns of CIV, PBCV-1, and PS pellets. While the anisotropic patterns reveal ordered arrangements for the CIV and PS nanospheres, PBCV-1 remains isotropic. We suspect that PBCV-1 is unable to self-assemble into ordered arrays, in agreement with the white aspect of the pellets (unlike the opalescent aspect of the other samples). Two reasons can account for this inability: (i) in contrast to CIV and WIV [30], PBCV-1 does not have a halo of fibers that protrude from the capsid; the interaction between the fibril halos of different virions is expected to play a major role in the self-organization, thanks to their interdigitization. (ii) Unlike the iridoviruses, PBCV-1 has a 34-nm protruding spike at one vertex of the icosahedron; this asymmetrical feature prevents long-range ordering.

Azimuthal averaging of CIV and PS are displayed in Fig. 3. The resulting curves reflect the product of the form factor $P(Q)$ of the individual virions (as measured with the diluted suspensions) with the structure factor $S(Q)$ that is inherent to the crystalline (or paracrystalline) order. The $S(Q)$ signatures correspond to the narrow Bragg peaks appearing on top of the form factor oscillations. The Q ratios of the Bragg peaks observed for both CIV and PS colloids most closely agree with that expected from a hexagonal close-packed (HCP) structure. The absolute Bragg peak values measured for CIV yield an average lattice parameter $a = 235 \pm 11$ nm; this value is in good agreement with in-plane inter-virion separations

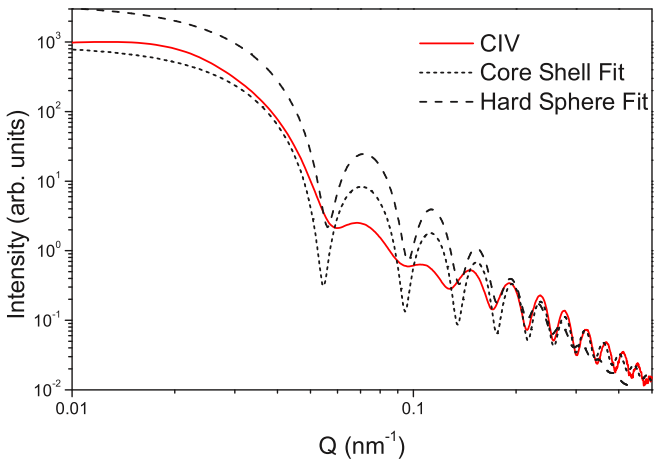

FIG. 1. (Color online) USAXS profiles and corresponding fits of (a) CIV, (b) PBCV-1, and (c) PS nanopsheres.

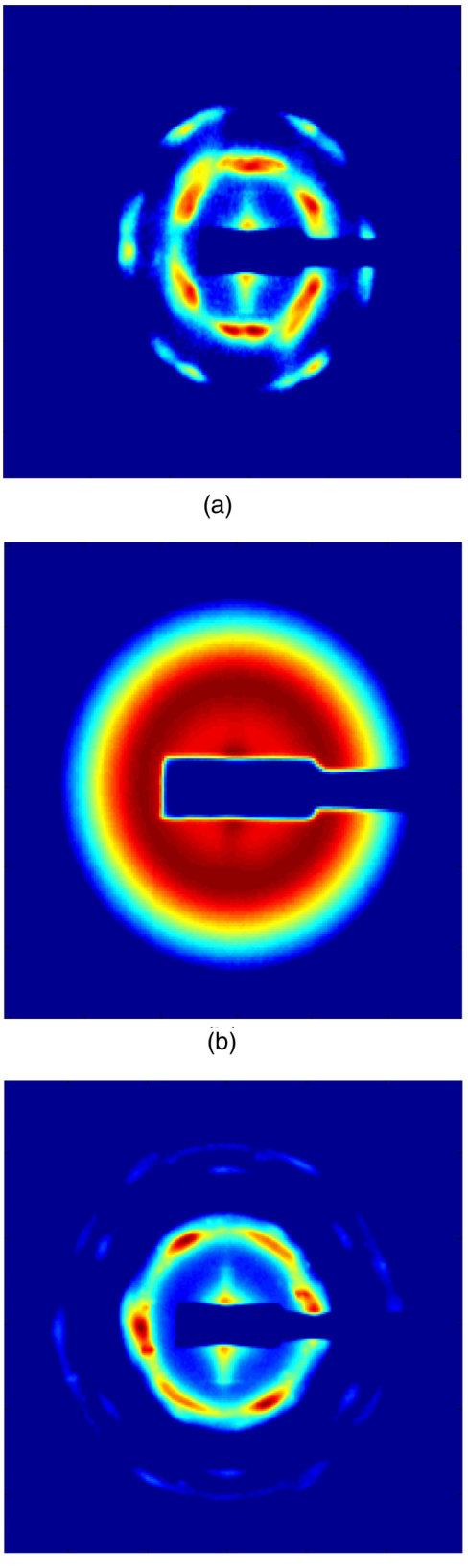

FIG. 2. (Color online) 2D USAXS patterns from wet pellets of (a) CIV, (b) PBCV-1, and (c) PS nanopsheres.

observed from micrographs of vitrified samples [27]. In the case of PS nanospheres, one finds $a = 215 \pm 8$ nm. It is worth noting that the ratios between the Q positions of the peaks are closer to ideal values of the HCP structure for PS nanospheres than for CIV. In addition, the 2D USAXS pattern of the PS pellets [Fig. 3(b)] has more narrow Bragg peaks. From these observations, one concludes that PS nanospheres form more regular and more extended arrays than CIV.

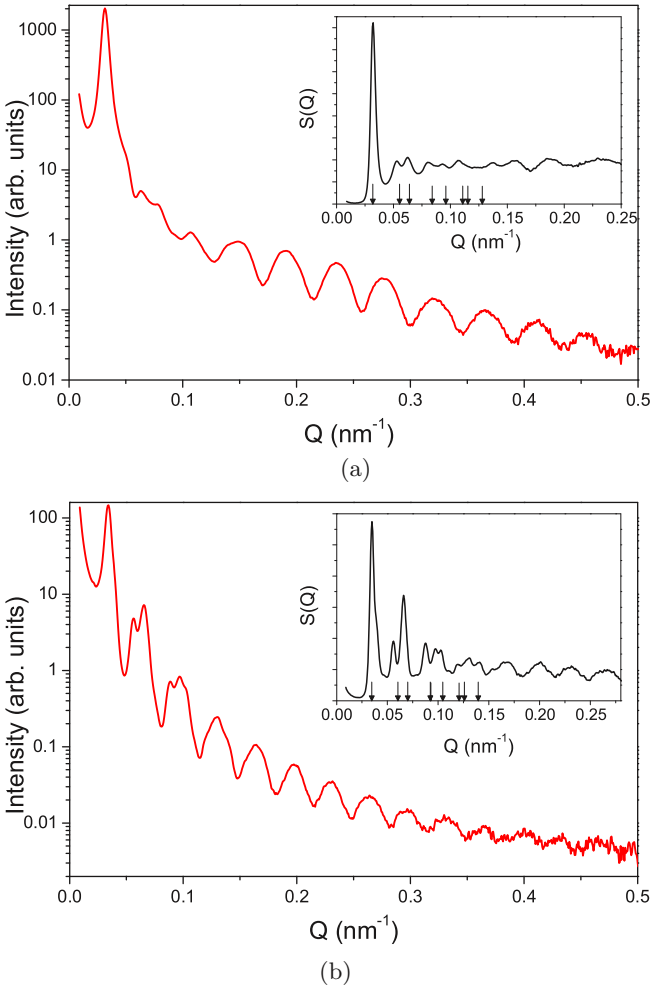

FIG. 3. (Color online) Azimuthally averaged USAXS profiles of (a) CIV and (b) PS pellets. Insets show the derived structure factors $S(Q)$. Black arrows mark the expected Q positions for a HCP layer arrangement ($1 : \sqrt{3} : 2 : \sqrt{7} : 3 : \sqrt{12} : \sqrt{13} : 4$).

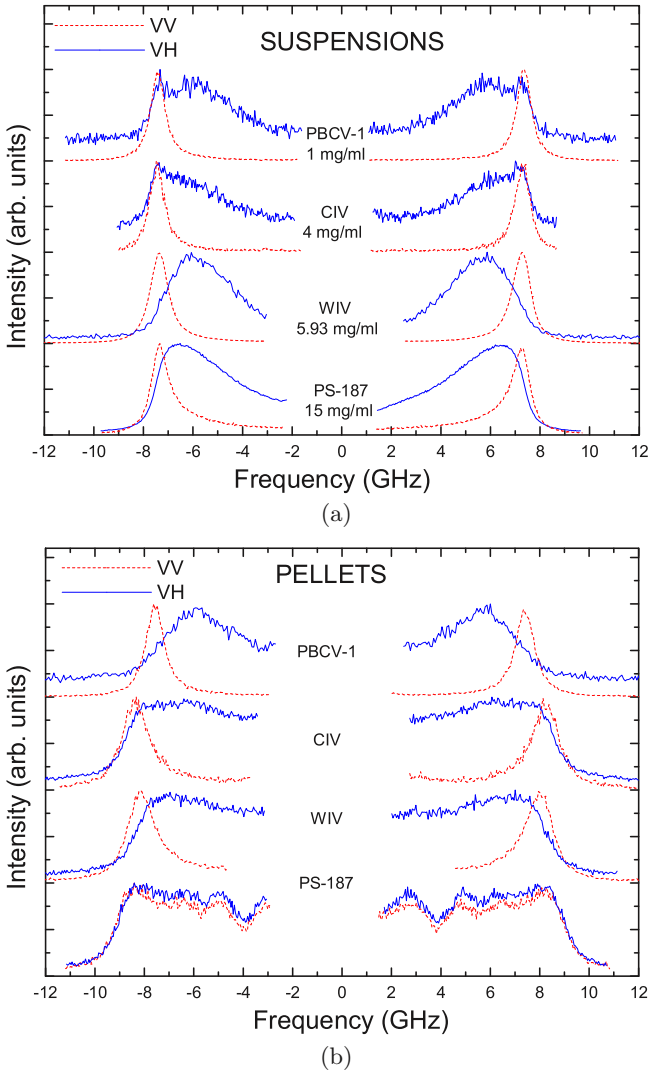

FIG. 4. (Color online) VV (solid line) and VH (dashed line) spectra of PBCV-1, CIV, WIV, and PS nanospheres (a) in suspensions, at the respective indicated concentrations (b) in pellets.

From the compared USAXS characterization of the three viruses with PS nanospheres, one confirms that viruses can be morphologically qualified as "biological nanospheres." As polymer colloids, they show high monodispersity, quasispherical morphology and are able, in the case of the two iridoviruses, to form well-ordered assemblies. These high-quality morphological aspects lead to postulate the existence of nanosphere vibration modes in viruses [24,32–35]. These modes have been demonstrated to exist and to be well probed in a variety of nanoparticle systems [10], including ordered assemblies of PS colloids [36–39]. In the following experiment, the same technique used to probe nanoparticle modes from PS colloids was used to explore their existence in CIV, WIV, and PBCV-1 particles.

B. Brillouin and Raman scattering

1. *Diluted suspensions* versus *pellets*

Figure 4(a) displays parallel (VV) and crossed (VH) polarization low-frequency spectra obtained from the milky suspensions of PBCV-1, CIV, WIV, and PS nanospheres. All spectra are normalized on the maximum intensity for clarity; however, real intensity maxima of parallel polarization spectra are typically ten times larger than those in crossed polarizations. All VV spectra exhibit an obvious sharp peak around 7.4 GHz. This frequency position nearly matches that of the Brillouin line from longitudinal modes in pure bulk water in the same experimental conditions [16]. It is thus assigned to the aqueous buffer.

In contrast to the VV spectra, the VH spectra of the solutions display a broadband, centered about 6 GHz, together with a trace of the aqueous buffer signal in the case of the less concentrated samples. This broadband arises from multiple scattering in the turbid samples, irrelevantly of both the size and the nature of the particles that cause the turbidity; it cannot be interpreted as a Raman signal from nanoparticle modes. Indeed, according to the elastic sphere model [10], low-frequency Raman scattering from nanoparticle modes is expected to scale with the inverse diameter of the nanoparticles and with the sound velocity inside the nanoparticle according to $\nu \approx v_{\text{sound}}/D$. Comparing different virus sizes like CIV

($D \simeq 190$ nm) and WIV ($D \simeq 140$ nm), with expected comparable sound velocities, one should therefore observe a significant frequency shift of the low-frequency signal, which is clearly not the case. Furthermore, no shift is observed comparing the broadband signal of the nearly identical size CIV (or PBCV-1) and PS colloids, although they are expected to have different sound velocities. Definitely, the most sound interpretation of the poorly defined broadband observed near 6 GHz for all samples is an effect of multiple scattering in the turbid samples, which results in scattering from all wave vectors ranging between zero and the maximum one transferred in backscattering configuration. This upper frequency soft cutoff is well consistent with the frequency position of the Brillouin signal from the aqueous buffer observed in VV configuration. In accord with its multiple scattering origin, the broadband was observed to increase in intensity with increasing the particle concentration, hence with increased turbidity (while at the same time the VV signal from the aqueous buffer decreased); besides, the broadband remained unchanged upon changing the scattering geometry.

For comparison with the suspensions, Fig. 4(b) shows the VV and VH spectra from the highly concentrated pellets. Qualitatively, both VV and VH spectra from the virus samples are very close to those observed in the suspensions, i.e., a bulk water-like spectrum in VV and a broadband in VH conditions, with a somewhat noticeable increase of scattering toward zero frequency; this increase is consistent with a larger turbidity of the pellet samples. As for the PS samples, one observes that VV and VH spectra are nearly identical, with no more trace of bulk aqueous buffer in parallel polarizations. Instead, for both polarizations, substructures are seen to emerge out of the broadband. As will be seen further, these substructures turn out to be presignatures of the PS nanosphere eigenmodes, as the pellets are dried. The absence of comparable substructures for virus pellets leads us to conclude that, although they structurally resemble hard-sphere colloids (as revealed by USAXS), they do not behave as such from a vibrational point of view. To determine if the still significant water content in the virus pellets was responsible for not detecting nanoparticle modes in the virus samples, the evolution of the broadband signal was investigated during drying.

2. *Evolution of the VH broadband during drying*

Starting from wet pellets of PS colloids placed in between coverslips, a series of VH spectra were recorded as a function of time during which water progressively evaporated (the excitation power was increased to 40 mW). Figure 5 shows the evolution of the spectra recorded at regular time intervals of 5 min. For both systems, one clearly observes the pellet "continuum" broadband progressively turning into a discrete spectrum featuring the eigenmodes of the PS nanospheres as the pellets dry out.

The assignment of the peaks observed in the dry state [top spectrum in Fig. 5(a)] for PS nanospheres having sizes comparable to the one studied herein has been extensively studied and rationalized by Montagna *et al.* and Fytas *et al.* [36–39]. The observed modes are spheroidal Lamb modes (noted S_ℓ^n), characterized by the angular momentum ℓ and harmonic index n. For the present particles, essentially three

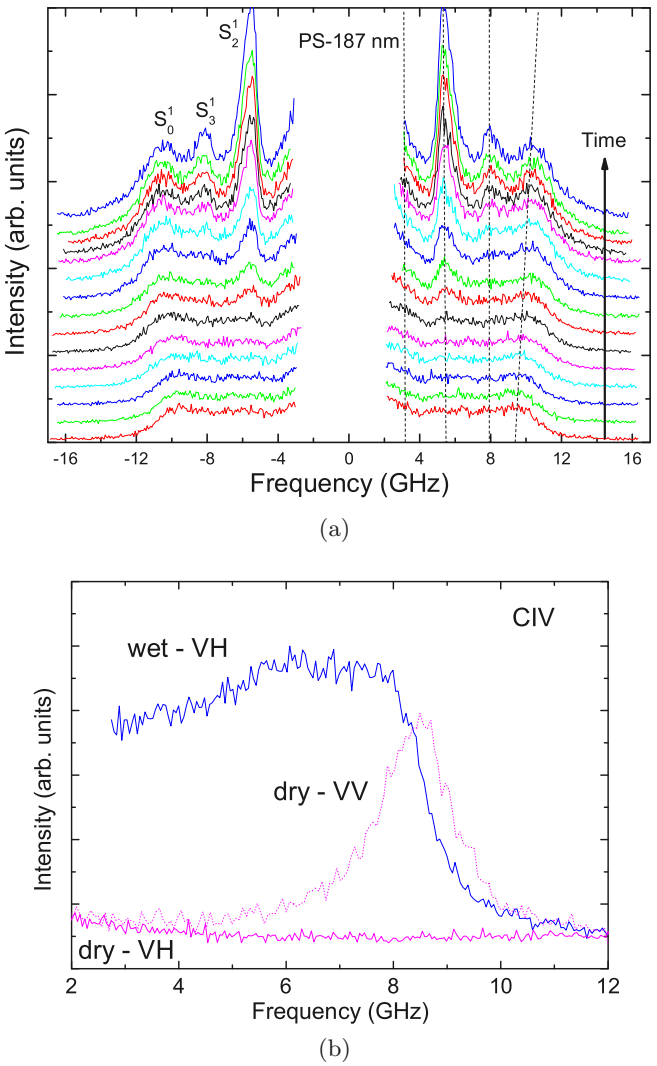

FIG. 5. (Color online) Evolution upon drying of the spectra from pellets of (a) PS nanospheres-VH, (b) CIV, VH (solid line) and VV (dashed line); the VV intensity was downscaled to be compared to the VH spectra.

modes contribute to the spectrum in the dry state: the most prominent mode is the fundamental of the quadrupolar mode, S_2^1, followed by the S_3^1 and S_0^1 modes (with a minor contribution of the S_2^2 mode in the vicinity of the latter one), with respective increasing frequencies.

When comparing the wettest state and the driest state, it is difficult to find presignatures of the eigenmodes in the wettest pellet spectra, except for the S_0^1 mode, which seems to correspond with the high-frequency soft cutoff observed for the wet pellets. However, this correspondence was observed to be size-dependent (data not shown): the same cutoff matches with another eigenmode (S_4^2) for PS nanospheres of about 300-nm diameter. Definitely, what appears as the most reliable early signature of a nanosphere eigenmode is the S_2^1 mode, which is the first peak to emerge out of the broadband during the drying. Finally, it is interesting to notice the behavior of the scattered intensity between 2 and 4 GHz (due to the strong quasielastic scattering of the samples, it was not possible to reach frequencies lower than 2 GHz). It was recently demonstrated [39]

that this ultra-low frequency region features the contribution of the S_1^1 Lamb mode whose frequency goes off from zero upon coupling between the nanoparticles ($\nu_{S_1^1} = 0$ for free nanospheres); the stronger the coupling, the more the ultra-low frequency shoulder is shifted toward higher values. Qualitatively, a similar trend is observed in Fig. 5(a): what can be interpreted as the high-frequency tail of a quasielastic shoulder lying below 2 GHz in the wettest state turns to a better-defined shoulder at midpoint through drying. Beyond this point, the intensity of the nanosphere eigenmodes progressively dominates, at the expense of the quasielastic shoulder. This evolution implies that throughout the early stages of drying, the interaction between the particles grows until the interaction decreases due to the complete evaporation of the solvent.

Monitoring the effect of drying with the virus pellets proves hard pressed. Indeed, due to the very low virus concentrations and probably to a lower scattering efficiency compared to PS, recording the VH spectra with the virus pellets requires very large acquisition times (several hours versus several minutes for the PS pellets). Over such long acquisition times, the virus pellets certainly dry off so that the spectra shown in Fig. 4(b) reflect an average situation between freshly wet and nearly dry. Figure 5(b) shows the obtained results for CIV as an example: once the pellet is completely dry, i.e., after several hours of VH recording, the VV spectra show a single narrow band, which can safely be assigned to a longitudinal mode within the dried pellet. Accordingly, this band is suppressed in VH conditions and no further signal can be detected. Obviously, unlike the PS pellets, no nanoparticle mode can be found in the dry virus pellets.

3. *Structural characterization after drying*

The fact that after drying the spectra of the virus pellets do not show nanoparticle modes may be interpreted as a disruption of the virions. In order to check the state of the virions after drying, TEM characterizations were performed on WIV, CIV, and as a comparison, on the PS colloids (Fig. 6). A further 3D AFM characterization was performed for CIV.

Both TEM and AFM observations confirm that the overall integrity of the virions is conserved after drying: all images display well-defined contours of the particles with sizes and size distributions that conform to the expected ones. The AFM picture of the CIV pellet shows the densely packed arrangement of the viruses with a granularity that matches the CIV sizes. One essential difference between the virus samples and the polymer nanospheres is the sharp contrast observed in the latter. Besides, wherever particles aggregate, the contact between the particles appears tighter between virions than between PS nanospheres, as can be seen from the voids in between them.

IV. DISCUSSION

According to our results, no trace of nanoparticle mode can be found for the studied viruses, at least when looking at virus assemblies such as pellets, unlike the polymer colloid counterparts. Several explanations can be found for this nonobservation.

As described above, the model used to estimate the frequencies of the virus nanoparticles modes is the elastic

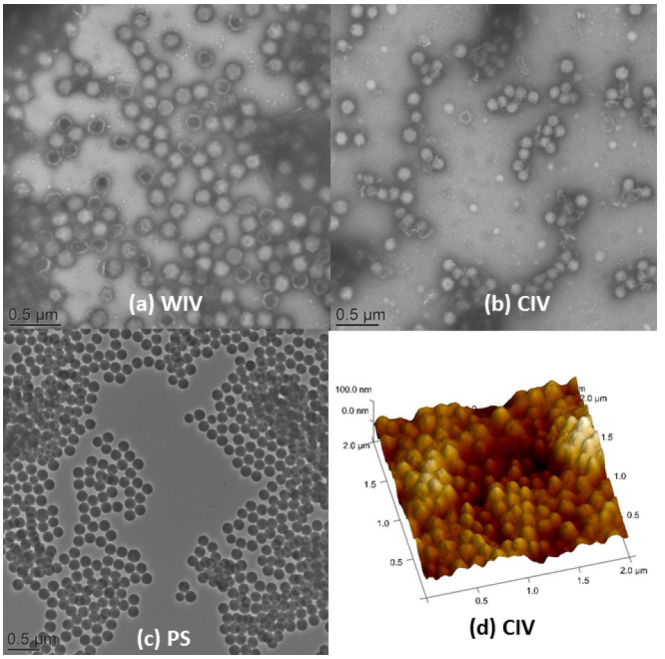

FIG. 6. (Color online) TEM characterization of (a) WIV, (b) CIV, and (c) PS nanoparticles after drying. CIV and WIV micrographs were obtained in negative staining. (d) AFM characterization of a dried CIV pellet.

sphere model, which is generally thought as more appropriate because of the relatively strong stiffness of viral capsids [16,22,32,35]. Applying this model to a virus of 190 nm, i.e., using elastic constants that are typical of viral matter [16], yields spheroidal mode frequencies of 4 GHz for the quadrupolar S_2^1 mode and 9 GHz for the breathing S_0^1 mode. These values are expected to hold even in the case of slightly faceted nanoparticles (like viruses), as demonstrated for solid nanoparticles with polyhedral faceted shapes departing from a sphere [40]. Out of these two modes, theoretical calculations [24,41] estimated that the quadrupolar mode should be the least damped one due to the interaction with the solvent. For virus sizes between 190 and 140 nm, one therefore expects to detect quadrupolar modes between 4 and 6 GHz, or slightly lower due to damping. Although very low, this frequency range could be probed with the present experiment. As suggested by L. H. Ford [32], another model may be used to estimate the natural vibration frequencies of virions, namely the liquid drop model. Compared to the elastic model, the liquid drop model emphasizes more the liquid-like nature of the vibrating nanoparticle. The frequency values calculated from this model typically lie one order of magnitude lower than those estimated with the elastic sphere model, i.e., in a frequency range not accessible to our experiment; other interferometric devices would be needed to explore such ultra-low frequency domain.

If the elastic sphere model has proved to be a good evaluation tool of nanoparticle mode frequencies for solid spheres (hence including polymer colloids), its application to softer structures like viruses that are in strong interaction with the dynamical hydrogen bond network of water is less straightforward. One way to account for the softness of viral structures is to estimate the damping of the vibration modes,

which in general causes linewidth broadening and downshift of the mode frequencies [23,42,43]. A first estimate of the damping situation can be can made by evaluating the acoustic impedance mismatch Z_{NP}/Z_{env}: for PS nanospheres in water, $Z_{PS}/Z_{H_2O} \simeq 1.7$, while for viruses in water $Z_{virus}/Z_{H_2O} \simeq 1.3$, taking for viruses a mass density identical to that of water and $v_L = 1920$ m/s [16]. Obviously, damping effects are most severe for the substantially softer viruses, an aspect not reflected by the USAXS characterization. Murray *et al.* [41] numerically evaluated the damping of soft viruses vibrating against a water-embedding medium using the complex frequency method. They showed that the breathing S_0^1 mode is severely damped ($\omega\tau \ll 1$) while the quadrupolar S_2^1 mode is at the limit of damping ($\omega\tau \simeq 1$). Dykeman *et al.* [24] confirmed that less symmetric modes from spherical capsids like the S_2^1 quadrupolar mode should be the least damped of the spheroidal modes. Yet, according to our experimental observations, no such damped mode could be identified in the low-frequency Raman or Brillouin spectra. Reducing the damping by minimizing the water content through centrifugation proved ineffective, as well as further drying of the virus pellets although the virions were shown to keep a well-defined morphology after drying. These results contrast with a previous study reporting a weak signal from monolayers of WIV deposited on a silicon substrate, in a dry state [18]. Differently from this study, the samples investigated herein consist of centrifuged pellets inside which the viruses are densely packed, as unveiled by the AFM characterization [Fig. 6(d)]. Comparatively, dry PS opal structures show much less contact between the particles [37]. In the presence of a strong interaction [44], the delocalization of the eigenmodes acts as severe damping, so that vibrations cannot be considered any more as confined on the nanoparticles; instead, a delocalized longitudinal mode [such as that observed in Fig. 5(b)] propagates throughout the protein assembly, as if the viral structures were acoustically transparent. In the case of CIV and WIV, this interaction most likely originates in the interdigitization of the fibrillar structures, which is not expected to occur in PBCV-1, as confirmed by the USAXS studies. From these considerations, it could be that the pellet spectra observed with PBCV-1 might be the most workable ones in further studies.

The main outcome from our Brillouin and Raman study is that in spite of strong morphological and structural similarities with polymer nanospheres, viruses, at least when observed as assembled in the form of weakly wet opals, do not show nanoparticle modes. Possible reasons related to the poor quality factor of such modes were given in the above discussion. It is finally also worth questioning the very existence of virus eigenmodes. Indeed, most theoretical reports dedicated to virus particle modes refer, in fact, to the eigenmodes of the capsid [14,15,20,21,24], which is the most solid-like structure in virus particles. Although compact, morphologically well-defined, viral nanoparticles have complex inner structures. Heterogeneous elasticity [45–47] and/or diffuse structures of the several constituents (genome core, lipid layer, etc.) can prevent the development of motional coherence, which is a basic ingredient of nanoparticle modes. In this respect, it could be that a rigid uniformization of the capsid through crosslinking of its constituents would improve the situation. Note that the choice of ds-DNA viruses in which the genome is known to be highly pressurized [48,49] and, as a consequence, a more solid-like behavior can be expected, did not turn out to be efficient.

V. CONCLUSION

This study aimed to determine how the concept of "nanospheres," as understood from a solid-state point of view, could apply to large spherical-like viruses. To this end, PBCV-1, CIV, and WIV were compared with a PS colloid of comparable size. Morphological characterization provided by USAXS confirmed that these three large viruses can be correctly considered as "nanospheres" because they behave like polymer colloids in terms of morphology (shape definition, very low size dispersity) as well as their ability to self-assemble into ordered opal structures (except for PBCV-1). However, when it comes to the vibrational behavior, the hydrated viruses, in spite of the favorable ingredients like high morphological definition, cease to behave as solid nanospheres because they are unable to confine vibrations, unlike the polymer colloid counterparts. Possible reasons for this different behavior, like mechanical heterogeneity within the virus structure or unfavorable acoustic mismatch due to the presence of water, were discussed. Additional experiments using more uniformly rigid virus structures, e.g., after crosslinking, or studying procapsid structures with known, very differing elastic constants, may be warranted.

ACKNOWLEDGMENTS

A.M. and S.S. thank François Morlé for his help in the pellet productions, as well as Shirely Callow for the USAXS measurements. A.M. also thanks Hélène Gehan and Armel Descamps for their help in the TEM and AFM characterizations, respectively. This research was partially supported by NSF-EPSCoR Grant No. EPS-1004904 (JLVE) and NIH Grant No. P20 RR15635 from the COBRE Program of the National Center for Research Resources (JLVE). V.W. thanks Vivienne Young for technical assistance.

[1] X. Dang, H. Yi, M.-H. Ham, J. Qi, D. S. Yun, R. Ladewski, M. S. Strano, P. T. Hammond, and A. M. Belcher, Nat. Nano **6**, 377 (2011).

[2] A. A. A. Aljabali, J. E. Barclay, G. P. Lomonossoff, and D. J. Evans, Nanoscale **2**, 2596 (2010).

[3] Y. S. Nam, H. Park, A. P. Magyar, D. S. Yun, T. S. Pollom, and A. M. Belcher, Nanoscale **4**, 3405 (2012).

[4] E. Dujardin, C. Peet, G. Stubbs, J. N. Culver, and S. Mann, Nano Lett. **3**, 413 (2003).

[5] M. Young, W. Debbie, M. Uchida, and T. Douglas, Annu. Rev. Phytopathol. **46**, 361 (2008).
[6] Y. G. Kuznetsov and A. McPherson, Microbiol. Mol. Biol. Rev. **75**, 268 (2011).
[7] N. A. Ranson and P. G. Stockley, *Emerging Topics in Physic Virology* (Imperial College Press, London, 2010), Chap. 1, pp. 1–34.
[8] W. H. Roos, R. Bruinsma, and G. J. L. Wuite, Nat. Phys. **6**, 733 (2010).
[9] M. G. Mateu, Virus Res. **168**, 1 (2012).
[10] L. Saviot, A. Mermet, and E. Duval, in *Handbook of Nanophysics*, edited by K. Sattler (Taylor and Francis, London, 2010), Chap. 11, p. 11.
[11] A. Courty, A. Mermet, P. A. Albouy, E. Duval, and M. P. Pileni, Nat. Mater. **4**, 395 (2005).
[12] L. Saviot, D. Machon, A. Mermet, D. B. Murray, S. Adichtchev, J. Margueritat, F. Demoisson, M. Ariane, and M. d. C. Marco de Lucas, J. Phys. Chem. C **116**, 22043 (2012).
[13] H. Portalès, N. Goubet, L. Saviot, S. Adichtchev, D. B. Murray, A. Mermet, E. Duval, and M.-P. Pileni, Proc. Natl. Acad. Sci. USA **105**, 14784 (2008).
[14] F. Tama and C. L. Brooks III, J. Mol. Biol. **318**, 733 (2002).
[15] F. Tama and C. L. Brooks III, J. Mol. Biol. **345**, 299 (2005).
[16] B. Stephanidis, S. Adichtchev, P. Gouet, A. McPherson, and A. Mermet, Biophys. J. **93**, 1354 (2007).
[17] K. T. Tsen, S.-W. D. Tsen, N.-T. Lin, J. G. Kiang, E. C. Dykeman, and O. F. Sankey, J. Biomed. Opt. **12**, 024009 (2007).
[18] R. D. Hartschuh, S. P. Wargacki, H. Xiong, J. Neiswinger, A. Kisliuk, S. Sihn, V. Ward, R. A. Vaia, and A. P. Sokolov, Phys. Rev. E **78**, 021907 (2008).
[19] E. Duval, A. Boukenter, and B. Champagnon, Phys. Rev. Lett. **56**, 2052 (1986).
[20] Z. Yang, I. Bahar, and M. Widom, Biophys. J. **96**, 4438 (2009).
[21] E. C. Dykeman and O. F. Sankey, Phys. Rev. Lett. **100**, 028101 (2008).
[22] P. de Gennes and M. Papoular, *Polarisation matière et rayonnement* (P.U.F., Paris, 1969), pp. 243–258.
[23] L. Saviot, C. Netting, and D. Murray, J. Phys. Chem. B **111**, 7457 (2007).
[24] E. C. Dykeman and O. F. Sankey, Phys. Rev. E **81**, 021918 (2010).
[25] M. V. Cherrier, V. A. Kostyuchenko, C. Xiao, V. D. Bowman, A. J. Battisti, X. Yan, P. R. Chipman, T. S. Baker, J. L. Van Etten, and M. G. Rossmann, Proc. Natl. Acad. Sci. USA **106**, 11085 (2009).
[26] Y. Kuznetsov, J. Gurnon, J. Van Etten, and A. McPherson, J. Struct. Biol. **149**, 256 (2005).
[27] X. Yan, N. H. Olson, J. L. Van Etten, M. Bergoin, M. G. Rossmann, and T. S. Baker, Nat. Struct. Mol. Biol. **7**, 101 (2000).
[28] X. Zhang, Y. Xiang, D. D. Dunigan, T. Klose, P. R. Chipman, J. L. Van Etten, and M. G. Rossmann, Proc. Natl. Acad. Sci. USA **108**, 14837 (2011).
[29] X. Yan, Z. Yu, P. Zhang, A. J. Battisti, H. A. Holdaway, P. R. Chipman, C. Bajaj, M. Bergoin, M. G. Rossmann, and T. S. Baker, J. Mol. Biol. **385**, 1287 (2009).
[30] S. Juhl, E. Chan, Y.-H. Ha, M. Maldovan, J. Brunton, V. Ward, T. Dokland, J. Kalmakoff, B. Farmer, E. Thomas, and R. Vaia, Adv. Funct. Mater. **16**, 1086 (2006).
[31] J. R. Sandercock, *Trends in Brillouin Scattering: Studies of Opaque Materials, Supported Films, and Central Modes* (Springer-Verlag, Berlin, 1982), Chap. 6, pp. 173–206.
[32] L. H. Ford, Phys. Rev. E **67**, 051924 (2003).
[33] L. Saviot, D. B. Murray, A. Mermet, and E. Duval, Phys. Rev. E **69**, 023901 (2004).
[34] V. A. Fonoberov and A. A. Balandin, Physica Status Solidi B **241**, R67 (2004).
[35] M. Talati and P. K. Jha, Phys. Rev. E **73**, 011901 (2006).
[36] W. Cheng, J. J. Wang, U. Jonas, W. Steffen, G. Fytas, R. S. Penciu, and E. N. Economou, J. Chem. Phys. **123**, 121104 (2005).
[37] W. Cheng, J. Wang, U. Jonas, G. Fytas, and N. Stefanou, Nat. Mater. **5**, 830 (2006).
[38] T. Still, M. Mattarelli, D. Kiefer, G. Fytas, and M. Montagna, J. Phys. Chem. Lett. **1**, 2440 (2010).
[39] M. Mattarelli, M. Montagna, T. Still, D. Schneider, and G. Fytas, Soft Matter **8**, 4235 (2012).
[40] L. Saviot and D. B. Murray, Phys. Rev. B **79**, 214101 (2009).
[41] D. B. Murray and L. Saviot, J. Phys.: Conf. Ser. **92**, 012036 (2007).
[42] J. Roh, J. Curtis, S. Azzam, V. Novikov, I. Peral, Z. Chowdhuri, R. Gregory, and A. Sokolov, Biophys. J. **91**, 2573 (2006).
[43] P. V. Zinin, J. S. Allen, and V. M. Levin, Phys. Rev. E **72**, 061907 (2005).
[44] M. Mattarelli, M. Secchi, and M. Montagna, J. Chem. Phys. **139**, 174710 (2013).
[45] M. M. Gibbons and W. S. Klug, Biophys. J. **95**, 3640 (2008).
[46] E. May, A. Aggarwal, W. Klug, and C. Brooks III, Biophys. J. **100**, L59 (2011).
[47] R. Zandi and D. Reguera, Phys. Rev. E **72**, 021917 (2005).
[48] W. M. Gelbart and C. M. Knobler, Science **323**, 1682 (2009).
[49] T. Wulfmeyer, C. Polzer, G. Hiepler, K. Hamacher, R. Shoeman, D. D. Dunigan, J. L. Van Etten, M. Lolicato, A. Moroni, G. Thiel, and T. Meckel, PLoS ONE **7**, e30133 (2012).